Arabian Journal for Science and Engineering (2020) 45:5769–5781
https://doi.org/10.1007/s13369-020-04560-0

RESEARCH ARTICLE-MECHANICAL ENGINEERING

Establishing a Correlation Between Residual Stress and Natural Frequency of Vibration for Electron Beam Butt Weld of AISI 304 Stainless Steel

Debasish Das[1] · Dilip Kumar Pratihar[2] · Gour Gopal Roy[3]

Received: 6 November 2019 / Accepted: 19 April 2020 / Published online: 1 May 2020

Abstract
Residual stresses developed during complex *multi-physics electron beam welding process* are usually detrimental to the joint integrity. Moreover, the natural frequencies of vibration are reported to decrease with an increase in stress value. Not much literature is available on the study of the changes in natural frequency of vibration due to welding stresses. Moreover, such analysis is limited to mathematical modeling and conventional welding processes. Thus, in the present study, residual stresses of the welds corresponding to different heat inputs are measured experimentally using *X-ray diffraction machine*. *A Polytec laser vibrometer–data acquisition system–LabView* assembly is used to experimentally determine the natural frequencies of vibration. The novelty of this study lies with the establishment of a correlation between the measured welding stress and natural frequency of vibration. Additionally, the experimentally obtained residual stresses have also been validated through FEM results with satisfactory agreement. Furthermore, a noble approach of stress estimation using the natural frequencies is proposed and tested successfully.

Keywords Welding residual stresses · Stress-stiffening effect · Natural frequencies · X-ray diffraction · FEM

List of Symbols

C_p	Specific heat
h	Maximum heat source spread along the plate thickness
I	Beam current
k	Thermal conductivity
$M1$	Mode one natural frequency of vibration
$M2$	Mode two natural frequency of vibration
$M3$	Mode three natural frequency of vibration
$M4$	Mode four natural frequency of vibration
q_v	Volume heat flux
Q	Total input power
Q_s	Net power acting on the surface
Q_v	Net power acting on the volume
T	Temperature
t	Time
U	Welding speed
V	Accelerating voltage
r_b	Beam radius at the workpiece surface
r	Instantaneous beam radius
RS_{IPP}	Residual stress obtained from input process parameters
RS_{NFV}	Residual stress obtained from natural frequency of vibrations
x, y, z	Space coordinates
γ_s	A surface coefficient
γ_v	A volume coefficient
η	Efficiency
ρ	Density
ψ	Angles for stress measurements
DAQ	Data acquisition
EBW	Electron beam welding
FFT	Fast Fourier transformation algorithm

✉ Dilip Kumar Pratihar
dkpra@mech.iitkgp.ac.in

Debasish Das
dd4311@gmail.com

Gour Gopal Roy
ggroy@metal.iitkgp.ac.in

[1] Indian Institute of Technology Kharagpur, Kharagpur, India

[2] Department of Mechanical Engineering, Indian Institute of Technology Kharagpur, Kharagpur, India

[3] Department of Metallurgical and Materials Engineering, Indian Institute of Technology Kharagpur, Kharagpur, India

FEM	Finite element model
GTAW	Gas tungsten arc welding
NDT	Nondestructive testing
SS	Stainless steel
XRD	X-ray diffraction

1 Introduction

Vibration is associated with biology, geology, structure, machine components and various aspects of human life. The study of frequency and vibration has been employed in various fields of applications, such as in the analysis of earthquake, failure detection in engines and turbines and design of nuclear reactors. In fact, a rise in the demand and the use of vibratory equipment had been witnessed in the last few years. As a result, the study of vibration properties and its associated natural frequencies of a material could be employed profitably in various R&D and industrial applications [1].

Moreover, welding had been reported to be a multiphysical complex process [2], because of the simultaneous occurrence of heat transfer, fluid motion, stress formation, etc. [3, 4]. This results in the joints being prone to failure [4]. Additionally, as one of the most popular high-energy welding techniques, electron beam welding (EBW) process is accompanied by the higher cooling rate and strong influence of Marangoni forces, Lorentz and buoyant forces [5, 6]. The integrity and quality of the joints under the influence of these complex conditions need to be assured through proper inspection to prevent any monetary losses, unwanted failure and loss of life. Hence, proper inspection of the welded joints is needed to minimize the defect and, thereby, obtain quality products, which also ensures safety. Among many methods of welding defect inspections, the nondestructive testing (NDT) methods offer certain advantages. It has been reported to evolve from a small-scale laboratory experiment to an essential industrial need [7]. Furthermore, the demand for the better quality products led to the need of various available NDT tests to ensure the quality, longevity, safety and reliability of products, available in the market [8].

Among many welding issues, residual stress is one of the prime concerns, as it is known to strongly affect the mechanical properties of the joint [9]. Non-uniform heating and cooling during EBW of steel plates lead to non-uniform thermal expansion and compression, resulting in the development of transient stress–strain distribution and plastic deformation [10, 11]. High stress is observed to promote brittle fracture, failure or stress corrosion cracking and reduction in buckling strength [12]. Paradowska et al. [13] reported the loss in performances in corrosion, fatigue, fracture and creep due to stress. It also depends on the weld geometry and input process parameters. Moreover, post-weld heat treatment does not always ensure a complete removal of stress [14]. As a result, accurate information of stress becomes important from the point of failure analysis. Residual stress was reported to be measured using X-ray diffraction (XRD) [11, 15], neutron diffraction method [13, 16], drill hole method [17, 18], high-energy synchrotron radiation [19], ultrasonic method [20], magnetic Barkhausen noise (MBN) approach [11, 21], etc. Among many different NDT methods, defect identification using X-rays gained popularity in various industries and research fields [8]. However, measurement of welding stresses is subjected to several difficulties. For example, the stress measurement was carried out at one point at a time. Moreover, these were subjected to restrictions on specific types of materials [2]. Additionally, in some stress measuring machines, the sample size was to be reduced as per the size of the stage of that machine. Furthermore, the measurement of residual stress at EBW heat-affected zone (HAZ) through XRD is extremely difficult because of the small size of the HAZ [11]. In addition, repetitions of experiments are required for the minimization of deviation observed in the data. As a result, the overall welding stress measurement becomes a time taking, expensive and hectic process.

As a result, the roles of different simulation models become significant in the prediction of stress, as it could avoid accidents [15] and minimize need for actual experiments, time and cost involved in the overall process [10]. Even though the stress analysis through simulation is not easy, computationally expensive and often very challenging, it has gained popularity due to its capability to deliver reasonably accurate results [2]. Stress in welding had been predicted by various researchers through simulations [10, 15, 18, 22–25].

The stress-induced changes, leading to changes in the structural response, may be defined as the *stress-stiffening effect* [2, 26]. Noticeable changes in the dynamic response of the structures were observed by Bezerra et al. [26], because of the presence of welding-induced residual stresses. The change in natural frequencies because of the welding residual stress-induced stress-stiffening effect was investigated by Vieira et al. [2]. Stress was reported in some of the literature to be the reason for the observed variation in natural frequency [2, 26, 27]. However, most of these investigations were associated with conventional welding techniques only. In fact, work on the change in natural frequencies due to stresses, developed in the weld for different ranges of heat input $\left(VI/U\right)$, where V, I and U represent the accelerating voltage, beam current and welding speed, respectively, has not been reported yet.

Jubb and Philip [28] correlated frequency, stiffness, stress and load for a variety of structures and observed a decrease in the stiffness and frequency as a result of instability in structures, due to application of load. Kaldas and Dickinson [29] developed a Rayleigh–Ritz approach-based model for the prediction of natural frequencies and different mode shapes during the vibration of a stress-induced rectangular plate.

They further estimated the applicability and accuracy of the model using numerical examples. Kaldas and Dickinson [27] also proposed a theoretical approach, which could demonstrate the influence of residual stress, developed during gas tungsten arc welding (GTAW) in rectangular plates on vibration characteristics and mode shapes. Finite difference techniques were also employed in order to find the stress pattern. Vieira et al. [2] studied the effect of welding residual stresses on the dynamic behavior of rectangular plates through the study of variation, occurring in the natural frequencies during GTAW using experiments as well as numerical modeling. The numerical model-predicted dynamic characteristics of plates were found to be accurate with the experimental results. The influence of weld residual stress on geometrical distortion and stress-stiffening effect was studied by Bezerra et al. [26] through both the experiments as well as Ansys results with a good agreement between them. They found significant effect of residual stress on the dynamic characteristics of structure. A general trend of decreasing natural frequencies due to welding was observed [2, 26–29].

Ferro et al. [15] carried out EBW of Inconel 706 plates. They developed a finite element model (FEM) to predict the thermal stress and validated experimentally through XRD results. The thermal and residual stresses were observed to depend strongly on the bead geometry and presence of microfissures. Deshpande et al. [10] simulated butt welding and post-weld heat treatment process of Inconel 718 plates using Sysweld and Abaqus FEM packages to predict residual stress, temperature profile etc., where Sysweld was found to offer the useful inbuilt features for welding simulations. Barsoum and Barsoum [22] used Ansys FEM package for the prediction of residual stress during welding. Fatigue and crack propagation were also studied using linear elastic fracture mechanics (LEFM) in order to correlate residual stress with fatigue loading. Their model was found to predict accurate results. Thermo-mechanical FEM analysis using Ansys package was carried out by [24] in order to study the nature of distribution of stress and distortion in butt weld of stainless steel samples. They found that the effect of longitudinal stress is more than that of the transverse one responsible for failure. Huo et al. [18] developed a thermo-elasto-plastic model for the simulation of EBW and electron beam local post-weld heat treatment (EBLPWHT) in order to study the temperature and stress field of BT20 titanium. They observed the longitudinal stress to be more than the transverse stress. They also reported a reduction in residual stress because of EBLPWHT. The influence of longitudinal residual stresses on weld failure was found to be more than the transverse stresses [30]. Dissimilar EBW of austenite stainless steel AISI 316(N) and ferritic–martensitic steel (P91) was performed by Javadi et al. [31]. They carried out round-robin measurement of residual stress using five commonly used stress measuring methods and found an overall agreement between them. Xu et al. [32] carried out LBW and GTAW welding of AISI 304 SS pipes. They observed good agreement between the experimentally measured and numerically predicted weld geometry, temperature profile and residual stress, based on which they reported LBW to outperform GTAW welding.

No significant literature is available on the study of the changes in natural frequency of vibration due to welding stresses. Moreover, such analysis is limited to mostly mathematical modeling and conventional welding processes. Thus, a correlation between the experimentally measured residual stress values and natural frequency of vibration for high energy-based EBW process has not been reported yet in the literature.

This gap in the literature is addressed in the present study, where the welding residual stresses corresponding to different process parameters are measured experimentally using *X-ray diffraction (XRD) machine*. *A Polytec laser vibrometer–data acquisition (DAQ) system–LabView* assembly is used to experimentally determine the natural frequencies of vibration. The aim of the present investigation lies with establishing a correlation between the EBW-induced welding stresses and natural frequency of vibration. Additionally, the welding stresses are validated through FEM.

The rest of the text is structured as follows: Sects. 2 and 3 deal with the details of the experiments conducted and that of the FEM simulations, respectively. Results are discussed, and conclusions are drawn in Sects. 4 and 5, respectively.

2 Experimental Procedure

2.1 EBW Setup

The experiments have been conducted using a 80 kV–150 mA–12 kW EBW machine, installed at IIT Kharagpur, India, by Bhabha Atomic Research Centre (BARC), Mumbai, India. A photograph of the EBW machine is depicted in Fig. 1a. A photograph of the welded sample is also shown in Fig. 1b, from which the desired samples for vibration analysis are obtained.

Please note that during welding, the accelerating voltage (V), beam current (I) and welding speed (U) are varied in the ranges of 60–70 kV, 80–94 mA and 750–1650 mm/min, respectively.

2.2 Sample Preparation

AISI 304 stainless steel plates with the dimensions of 55 mm × 80 mm × 5 mm have been welded using EBW process for different sets of input process parameters. From the final welded structure of dimensions: 110 mm × 80 mm × 5 mm, a thin rectangular strip of dimensions 110 ± 1.54 mm $\times 4 \pm 0.238$ mm $\times 0.64 \pm 0.08$ mm is cut using wire-EDM

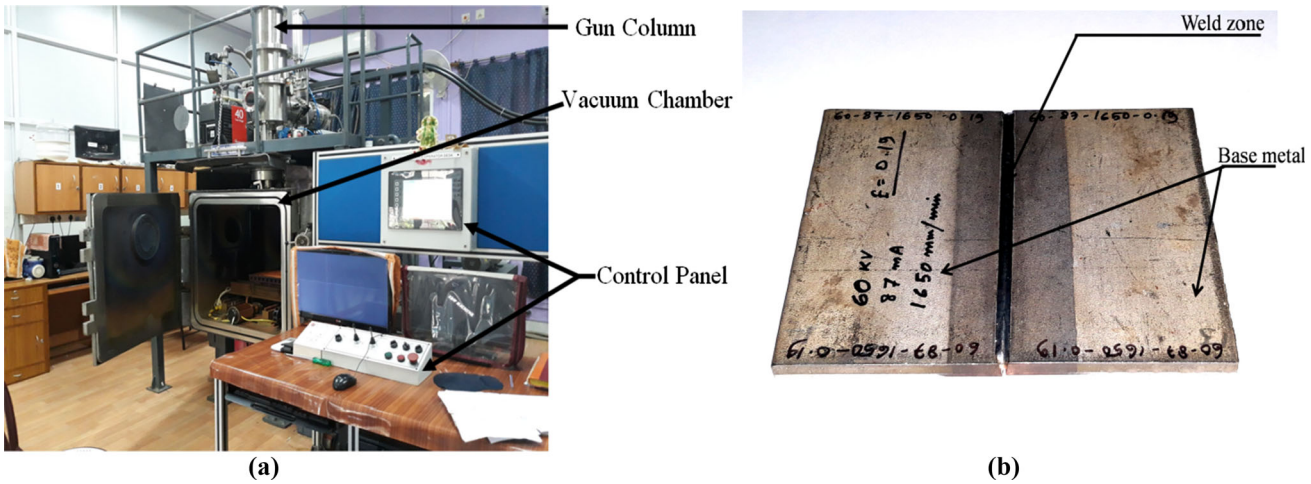

Fig. 1 **a** EBW setup at IIT Kharagpur, India, **b** EBW welded plates from which vibration samples are obtained

Fig. 2 Sample for determination if natural frequency of vibration

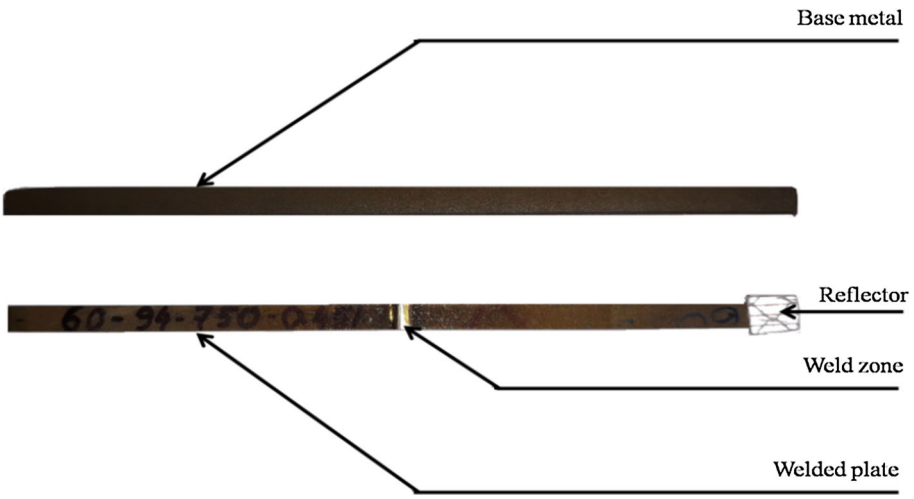

at Central Workshop, IIT Kharagpur, India. Figure 2 shows the sample used for the determination of natural frequency.

2.3 Determination of Different Modes of Vibration

The experiments for determining the natural frequency of vibration are carried out at the Systems, Dynamics and Control Laboratory, Department of Mechanical Engineering, IIT Kharagpur, India. During the experiment, a length of 5 mm is used to fix these thin samples on an anvil. A reflector is attached at the free end of the plate to reflect the laser light, coming from the PDV-100 Polytec portable digital laser vibrometer. The plate is struck manually and is then allowed to vibrate. This vibration is recorded directly in LabView 2012 using a DAQ system. The data acquisition system captures the experimental vibrations of the present problem in the form of velocity–time plot, and the frequencies are calculated using fast Fourier transformation (FFT) algorithm. These frequency data corresponding to different mode values are stored as *.m* MATLAB format file. The numerical values of the frequencies are directly obtained from these MATLAB files. These vibration data corresponding to different welding parameters have been analyzed. This is shown in Fig. 3. Here, Fig. 3a shows the simplified representation of the actual experimental setup, where vibration occurs along the z-axis. The actual complete experimental setup is shown in Fig. 3b. Please note that the changes in natural frequency of vibration are considered up to fourth mode. This is so, because of the unavailability of frequency information of mode 5 and above due to damping effect.

A block diagram, used in LabView software to obtain different modes of natural frequency, is shown in Fig. 4.

2.4 Stress Measurement

Stress measurements have been carried out using PANalytical EMPYREAN XRD machine, at Mechanical Engineering Department, IIT Kharagpur, India. The tube voltage and cur-

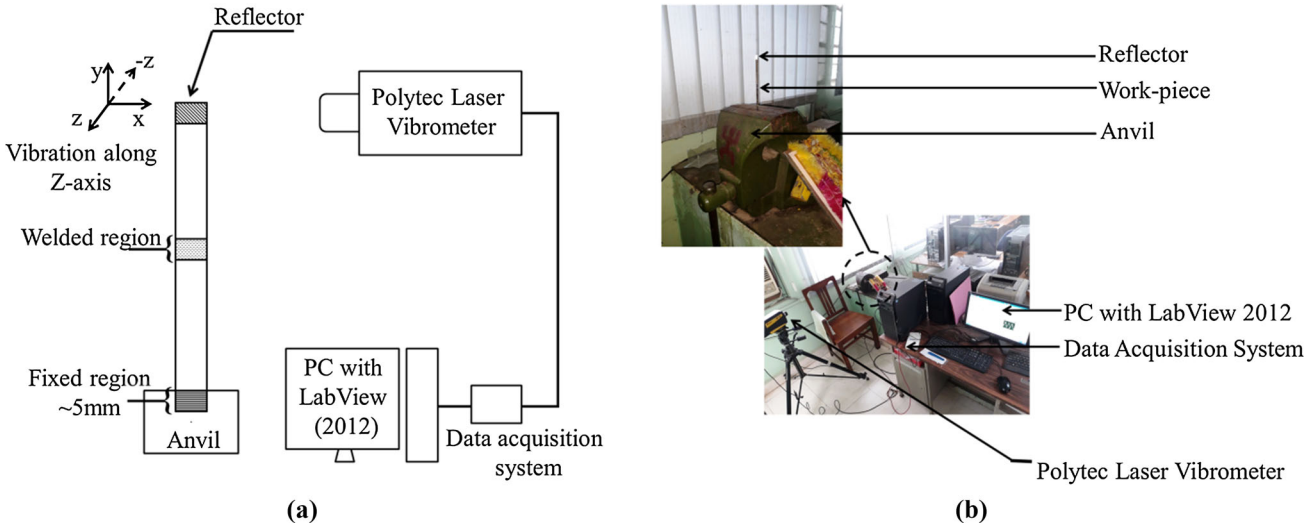

Fig. 3 **a** Simplified representation of the experimental procedure, **b** experimental setup for the measurement of frequency of vibration using fast Fourier transformation algorithm

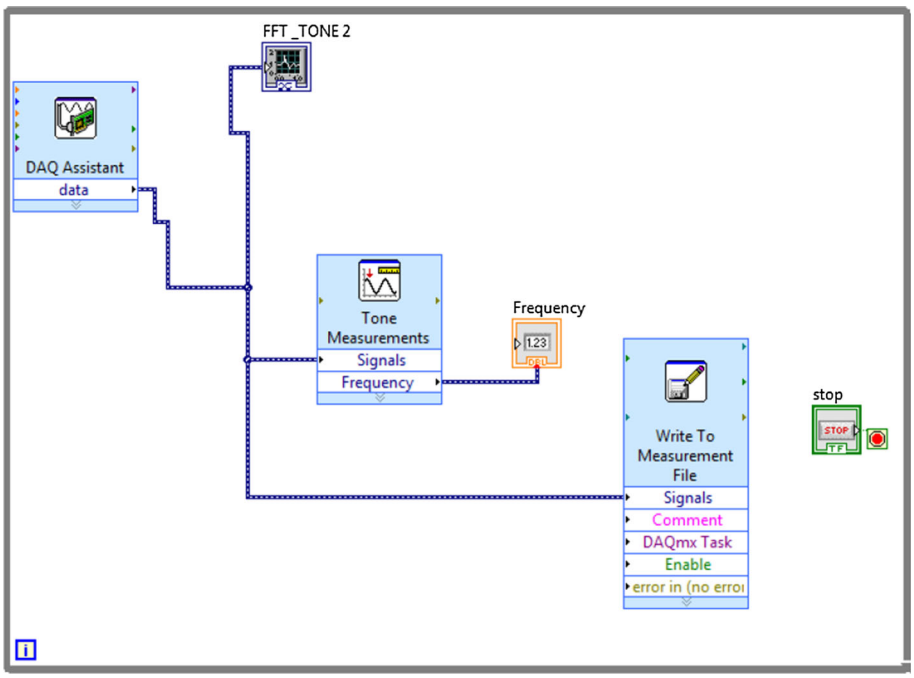

Fig. 4 Block diagram used in LabView 2012 software

rent are kept equal to 30 kV and 55 mA, respectively, for X-ray generation from chromium target. The sample has been scanned with CrKα radiation at $2\theta = 129^{\circ}$, corresponding to *hkl* plane {220}, as suggested in the literature [33]. The stress values have been analyzed through PANalytical stress plus 2.3 software employing $\sin^2(\psi)$ method [12, 15]. Please note that the measurement of stress values corresponding to a particular welding condition has been conducted three times at a point in the fusion zone, and their average is reported to ensure repeatability of the dataset. Moreover, only longitudinal stresses in the fusion zone are considered due to their more significant contributions to the failure of components compared to other stresses, as discussed in the literature [40, 41].

3 Estimation of residual stresses through FEM simulations

Rosenthal first proposed a model to represent a heat source [34, 35]. Henceforth, several 2D and 3D welding heat source models had been proposed. In particular, Goldak's double ellipsoid model [36] and deep penetration conical models

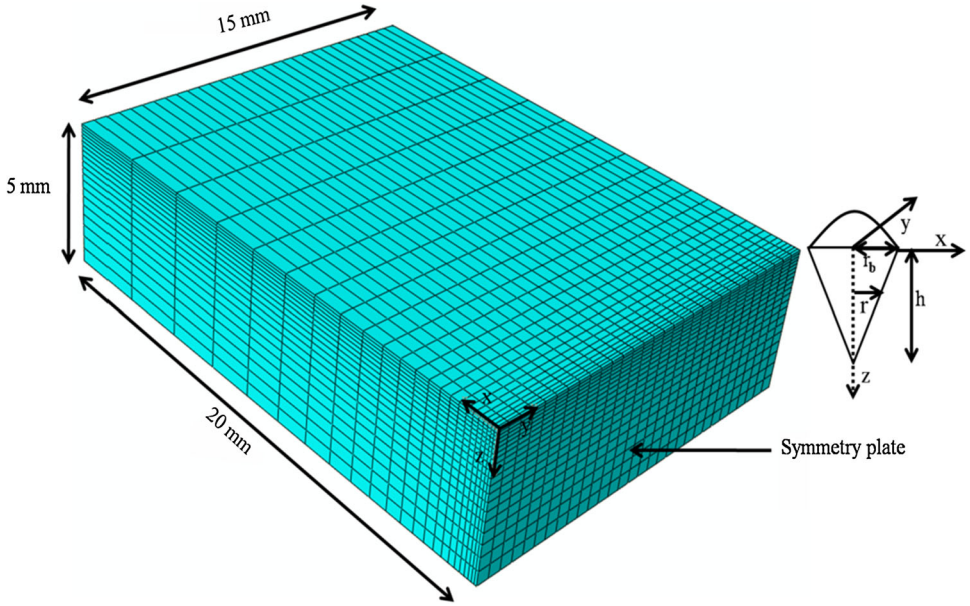

Fig. 5 Mesh distribution and employed beam profile used in of the present study

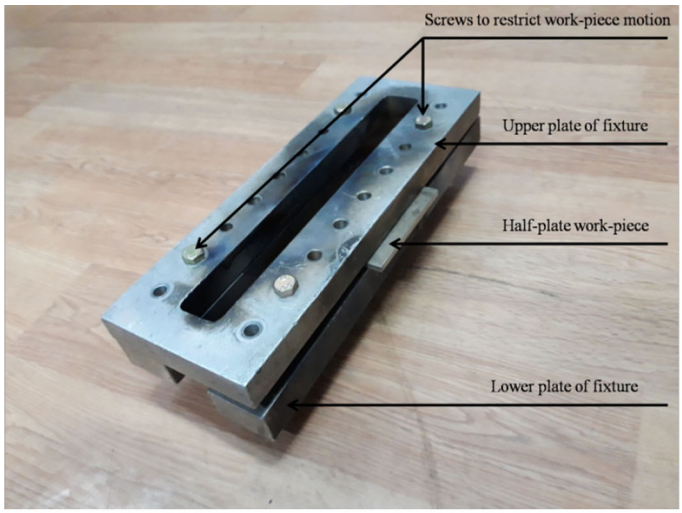

(a)

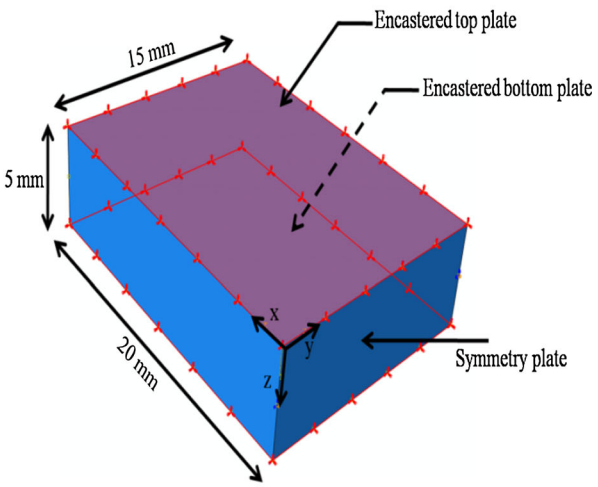

(b)

Fig. 6 Restraints applied to welding plate: **a** experimental top–bottom fixture setup, **b** FEM top–bottom encastre boundary condition

were used extensively [15, 37–40]. Phanikumar discussed many heat source models in NPTEL video lectures [38].

In the present study, a sequential thermo-physical FEM is developed with Abaqus 6.14 to extract information related to thermal and stress distributions. The details of the process are discussed below.

3.1 The Thermal Model

This section deals with thermal modeling of the EBW process. Assuming the part to be isotropic and homogeneous with no heat generation, the heat transfer model of conduction is given in Eq. (1) [41]:

$$\rho C_{\mathrm{p}} \frac{\partial T}{\partial t} = \frac{\partial}{\partial x}\left(k\frac{\partial T}{\partial x}\right) + \frac{\partial}{\partial y}\left(k\frac{\partial T}{\partial y}\right) + \frac{\partial}{\partial z}\left(k\frac{\partial T}{\partial z}\right), \qquad (1)$$

where the different space coordinates are denoted by the x, y and z coordinates. ρ, C_{p}, T, k and t have been defined earlier in the nomenclature table. This model also includes the heat losses through convection and radiation. The numerical values of the coefficient of convective heat transfer and emissivity are considered to be equal to 15 W/m^{2}K and 0.9, respectively [42].

Table 1 Material properties considered in the present analysis [5, 43]

Properties	AISI 304 stainless steel
Density of liquid (kg/m^3)	7200
Solidus temperature (K)	1697
Liquidus temperature (K)	1727
Specific heat (J/kg-K)	800
Coefficient of thermal expansion (1/K)	1.96E−05
Emissivity of the material	0.9

Table 2 Thermal conductivity and latent heat considered in the present analysis [25, 43–47]

Temperature (K)	Thermal conductivity (J/m s K)	Latent heat of fusion (kJ/kg)
293	25	247
1697	40	
1727	65	
3090	532.85	

Table 3 Temperature-dependent Young's modulus and Poisson's ratio used in the present study [48]

Temperature (K)	Young's modulus (GPa)	Poisson's ratio
277	194	0.27
466	184	0.28
686	168	0.3
1080	130	0.33
1281	73	0.34
1430	2	0.34

Table 4 Hardening model parameters used in the present study [48, 49]

Temperature (K)	Hardening model parameters for power law obtained at 3% plastic strain from the stress–strain curve	
	Yield point (MPa)	Tangent modulus (MPa)
343	293	1440
373	250	1480
473	210	1500
573	181	1470
723	157	1380
873	147	1510
1073	129	833
1273	48	640

3.1.1 Part Design

A 20 mm × 15 mm × 5 mm half plate with symmetric boundary condition about the yz plane is developed. The thermal cycle involves heating followed by the cooling, the same as that of real experiments. DC3D8-type mesh with 15,624 nodes and 13,800 eight-node linear hexahedral elements is used in the present study. The minimum and maximum mesh sizes are measured to be equal to 100 μm and 2.933 mm, at the fusion line and part end, respectively. The details of the mesh information along with beam profile used in the heat flux equation are shown in Fig. 5.

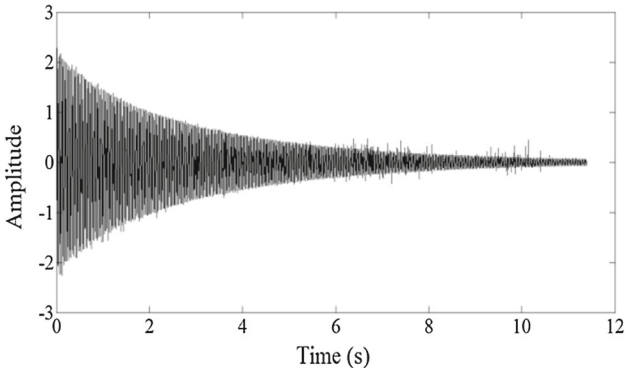

Fig. 7 Amplitude–time profile

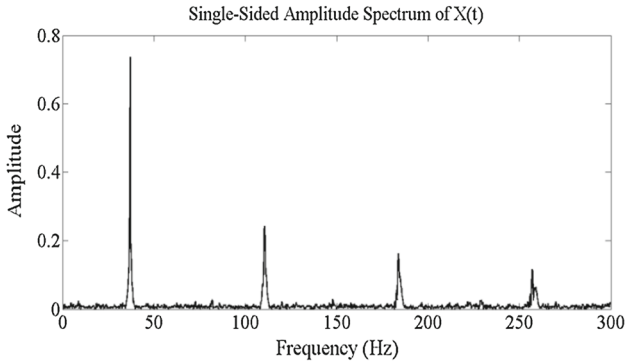

Fig. 8 Frequencies corresponding to different modes of vibrations

3.1.2 Heat Source Design

The conical heat source has been employed through DFLUX subroutine. The details of the volumetric heat flux equations along with mathematical formulations are available in the literature [39, 43]. Figure 5 also depicts the instantaneous beam radius (r) with respect to (x, y, z) space coordinates, as depicted in Eq. (2). This instantaneous beam radius (r) is considered to be the maximum on the workpiece surface (r_b), and it gradually decreases along the workpiece thickness, according to the considered conical heat source model. Moreover, the total input power (Q) is subgrouped into power acting on the surface ($Q_S = \gamma_S Q$) and volume ($Q_v = \gamma_v Q$), where the surface coefficient (γ_s) and the volume coefficient (γ_v) are considered to be equal to 0.1 and 0.9, respectively [39, 43]. Please note that being very small, the surface heat flux has not been considered in the present study. The net power con-

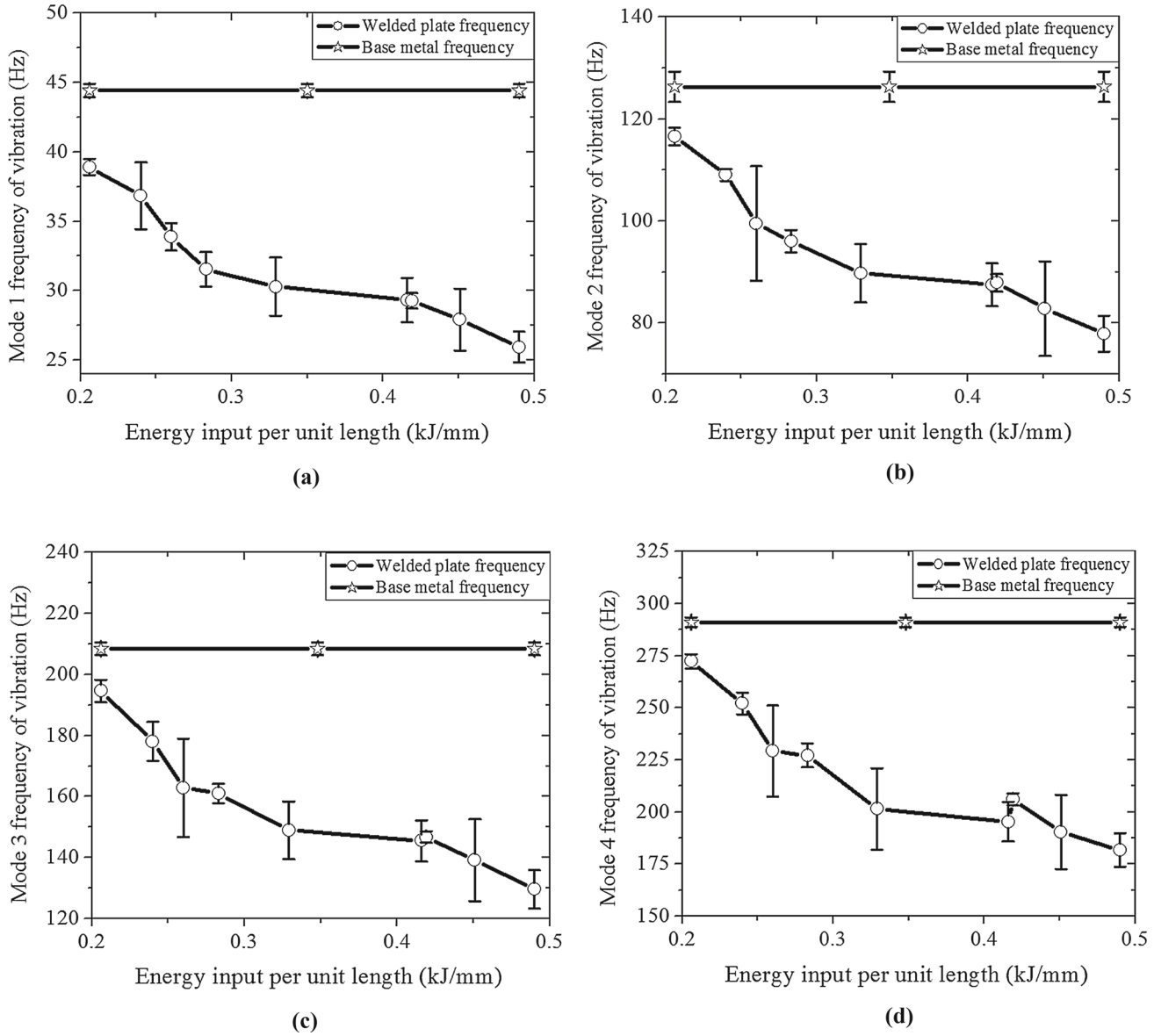

Fig. 9 Heat input versus natural frequency of vibrations corresponding to **a** mode 1, **b** mode 2, **c** mode 3, **d** mode 4

sidered is given in Eq. (3), where η, V and I are the efficiency, accelerating voltage and beam current, respectively. The volumetric heat flux is represented using Eq. (4), where q_v, r_b, h and z denote the volumetric heat flux, beam radius at the workpiece surface, maximum heat source spread along the plate thickness and instantaneous heat source spread along the plate thickness, respectively, as defined earlier:

$$r^2 = x^2 + y^2, \tag{2}$$

$$Q_v = \eta \gamma_v V I, \tag{3}$$

$$q_v(x, y, z) = \frac{9Q_v}{\pi r_b^2 h} e^{\left[-\frac{h^2}{(h-z)^2} \times \frac{3(x^2+y^2)}{r_b^2}\right]}, \tag{4}$$

As stated above in Eqs. (2–4), the instantaneous beam radius (r), volumetric power (Q_v) and volumetric heat flux (q_v) are essential to represent the incidence of the welding heat source (electron beam for the present study) on the workpiece. It is to be noted that these are well-established equations and are often reported in a different literature to represent conical heat source model in FEM analysis [39, 43].

3.2 The Mechanical Model

The temperature history has been used in the FEM mechanical modeling as inputs for estimation of the welding stresses. During experiments, fixtures are used to prevent the unnecessary workpiece movement. This is recreated in FEM model

using encastre boundary conditions at both the top and bottom surfaces of the half plate. This is done to keep the experimental and simulation boundary conditions as closely matching as possible, as shown in Fig. 6a, b, respectively.

3.3 Material Properties

The material properties, used in the thermal modeling of Abaqus 6.14, are listed in Tables 1, 2, 3 and 4.

Similarly, temperature-dependent Young's modulus and Poisson's ration are provided in Table 3 [48].

Moreover, Chakraborty et al. [48] observed kinematic hardening model to perform the better, and hence, it has been used in the present study. In addition, the temperature-dependent parameters of the hardening model, obtained using tangent modulus for the power law hardening curve obtained at 3% plastic strain from the stress–strain curve fitting, are provided in Table 4 [48].

4 Results

In this section, the authors first discussed about the changes occurring in the natural frequency of vibration with the corresponding change in the welding heat input. Next, the welding stresses, measured through XRD, are compared with the same, predicted through FEM results. Finally, a correlation between the natural frequency and welding residual stress is developed and discussed below.

4.1 Natural Frequency of Vibrations

In the present study, Figs. 7 and 8 show how the frequency dies out with time due to material damping. Figure 8 also displays that the decrease in amplitude with an increase in the frequency is almost exponential.

It has been reported in the literature that welding caused a decrease in the natural frequency of vibration [2, 26–29]. Our observations also are found to be in line with the literature. The natural frequencies of all the welded samples are observed to be less than that of the base metal. This reduction in the natural frequencies of vibration has been reported in the literature [2, 26, 27] due to the stresses developed in the weld. In addition, it has been observed that the natural frequency decreases with an increase in heat input. The correlation between heat input and natural frequency, obtained in the present study, is shown in Fig. 9.

4.2 Experiment Versus FEM-Predicted Stress in the Weld

The experimentally measured longitudinal residual stresses are observed to increase with heat input. This is in line with the observations, reported in the literature [15, 50, 51]. Moreover, the experimentally measured stresses closely matched the FEM-predicted results. The comparison among three different stress values, obtained experimentally and simulated through FEM, is shown in Fig. 10.

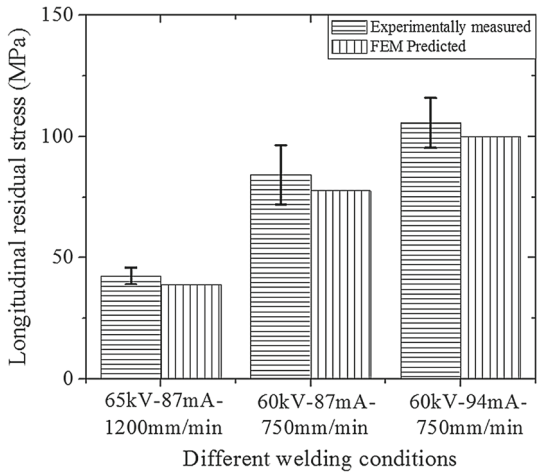

Fig. 10 Experimental versus FEM simulated stress values of the fusion zone corresponding to different welding conditions

4.3 Correlation of Natural Frequency with Welding Residual Stress

The natural frequencies of vibration up to mode 4 for all the welded joints are found to be less than that of the base metals (refer to Fig. 9). This is in line with the trend reported in the literature [2, 26–29]. Moreover, a reduction in the natural frequency is observed with an increase in heat input. Furthermore, the longitudinal residual stress in the weld is observed to increase with an increase in heat input. Hence, a correlation between measured natural frequencies, corresponding to different mode of vibrations and the welding stresses, measured using XRD process, is presented in Fig. 11.

It is observed from Fig. 11 that the stress and natural frequencies of vibration are inversely proportional. Hence, our investigation is in line with the expected trend available in the literature, that is, stress promotes damping through stress-stiffening effect.

4.4 Residual Stresses Prediction from the Natural Frequency of Vibrations

In the present work, the authors have also proposed a novel approach to predict the residual stresses, developed during the welding process from its natural frequency of vibration using regression equations. These equations are developed using Minitab 16. Please note that in the present study, linear regression equations have been used. The correlation coefficient (R^2) values of these linear equations are found to be

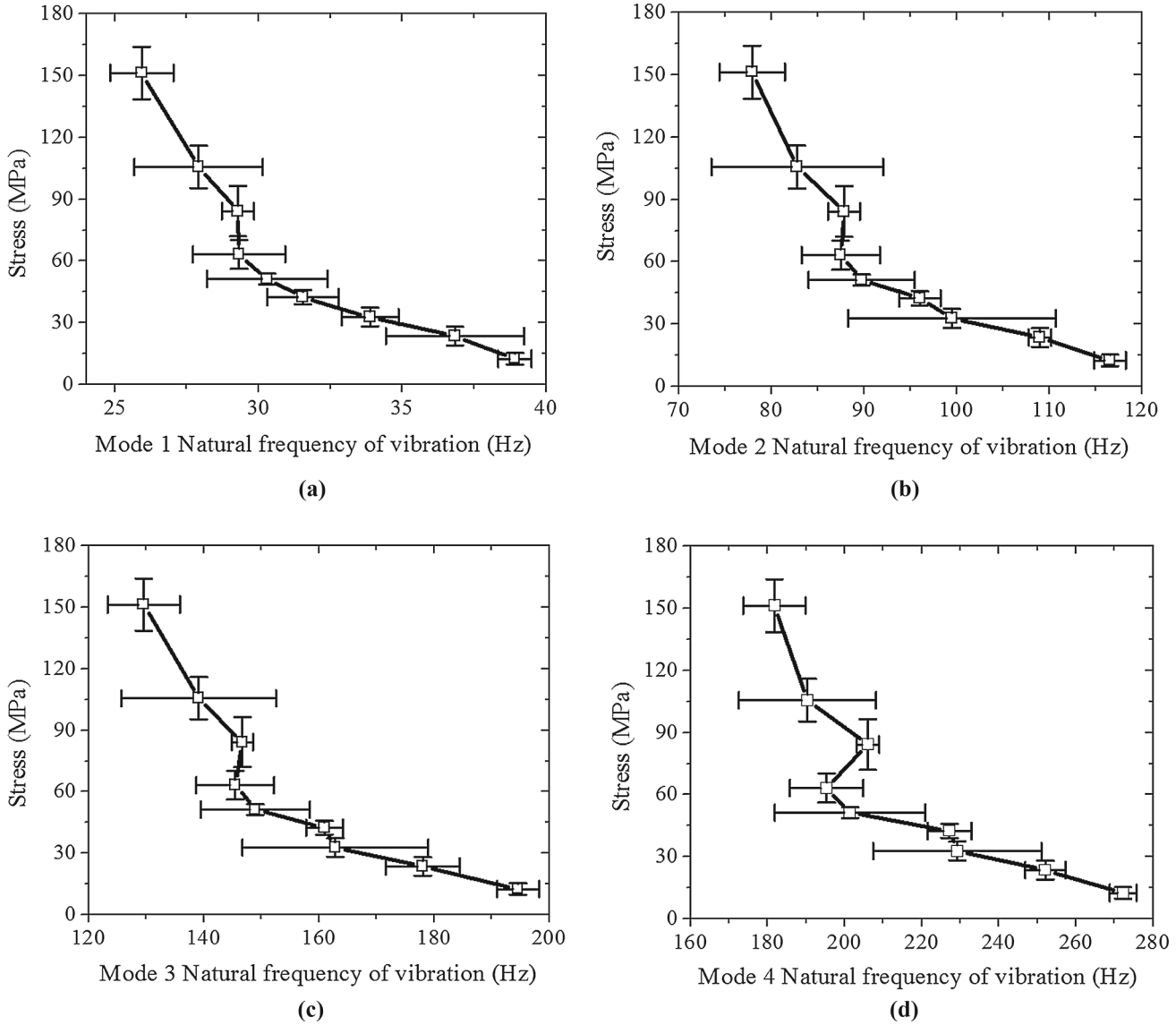

Fig. 11 Natural frequency of vibrations versus stress corresponding to **a** mode 1, **b** mode 2, **c** mode 3, **d** mode 4

around 90%. Moreover, these linear equations are found to yield better predictions compared to that of the nonlinear ones. As a result, they have been used in the present study (refer to Table 5). The predicted stress values using these equations are found to be in agreement with the corresponding welding stress value, measured experimentally through XRD. Equations (5)–(10) are provided in Table 5.

The input parameters are generated within their respective ranges by using random number generator. One thousand data have been generated using Eqs. (5)–(10). The stress values determined using the process parameters and the same, predicted using the modes of vibrations for the 1000 data, are shown in Fig. 12, which seems to have good agreement between them. This innovative approach of stress measurement is not only cost effective and easy to conduct but also is reliable and directly provides the stress values without using any complicated analysis. Hence, the stress of a structure could be predicted from the study of its structural behavior.

Table 5 Equations to represent natural frequency of vibrations and stresses

Equations	Eq. Nos.
$M1 = 51.1 - 0.289V - 0.164I + 0.0125U$	(5)
$M2 = 157 - 0.952V - 0.474I + 0.0374U$	(6)
$M3 = 273 - 1.86V - 0.725I + 0.0617U$	(7)
$M4 = 404 - 3.20V - 0.937I + 0.0945U$	(8)
$\mathrm{RS_{IPP}} = -113 - 0.17V + 3.36I - 0.100U$	(9)
$\mathrm{RS_{NFV}} = 391 + 22M1 - 22M2 + 1.4M3 + 3.84M4$	(10)

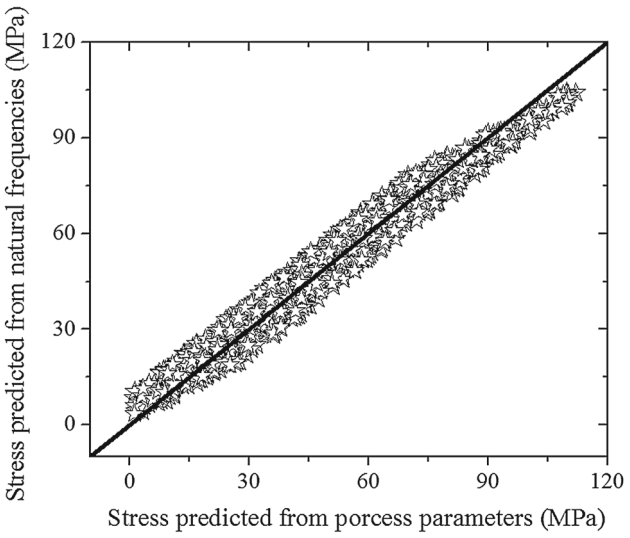

Fig. 12 Comparison of welding residual stress predicted using process parameters versus natural frequencies corresponding to different modes of vibration

This approach is new and has not been proposed to the best of the authors' knowledge.

It is important to mention that some minor deviations in the above-stated samples' dimensions are observed even after taking various precautions. This may be due to inherent limitations of the different employed experimental facilities, which include complexity of the EBW process, stress measurement through XRD, vibration analysis using vibrometer–DAQ system assembly, etc. However, the error has been minimized through multiple repetitions of the experiments.

5 Conclusion

The present study investigates the influence of welding residual stresses on the natural frequency of vibrations for a wide range of heat input. The natural frequencies of vibration corresponding to a given set of input parameters are measured and correlated to the longitudinal residual stress values measured using XRD at the weld fusion zone. The following conclusions have been drawn through the present study:

1. A novel approach of stress estimation using the natural frequencies of vibration is proposed in the present study.
2. Welding-induced residual stresses cause reduction in the natural frequency of vibration, which is in line with the literature.
3. The residual stress and natural frequencies are observed to increase and decrease, respectively, with an increase in the heat input. As a result, an inverse relationship between the natural frequency of vibration and residual stresses is observed.
4. The welding stresses measured experimentally through XRD and predicted through FEM simulations are found to be in close agreement between them.
5. Residual stress (RS_{NFV}) of the weld has been correlated to the natural frequencies of vibration ($M1, M2, M3, M4$) in the form of linear regression equation as:

$$RS_{NFV} = 391 + 22M1 - 22M2 + 1.4M3 + 3.84M4$$

Acknowledgements The authors are thankful to Prof. A. K. Samantaray, Systems, Dynamics and Control Laboratory, Department of Mechanical Engineering, IIT Kharagpur, India, for allowing us to use the digital laser vibrometer, LabView software and other setups required to carry out the necessary experiments on the measurement of natural frequency of vibration of welded samples. The authors are also grateful to the research scholars, namely Mr. Sebin Jose and Mr. Pankaj Kumar from the Systems, Dynamics and Control Laboratory, Department of Mechanical Engineering, IIT Kharagpur, India, for their immense assistance and support. The authors are also thankful to Mr. Surajit Mondal and the other members from DRDL, Hyderabad, India, for valuable insight into stress measurement. In addition, the authors are thankful to Prof. S. Paul, Department of Mechanical Engineering, IIT Kharagpur, India, for allowing me to conduct stress measurement.

References

1. Rao, S.S.: Mechanical Vibrations in SI Units, 6th edn. Pearson Education Inc., Hoboken (2017)
2. Vieira, A.B.; Rade, D.A.; Scotti, A.: Identification of welding residual stresses in rectangular plates using vibration responses. Inverse Probl. Sci. Eng. **14**, 313–331 (2006). https://doi.org/10.1080/17415970500521361
3. Feng, S.; Zhou, H.; Dong, H.: Using deep neural network with small dataset to predict material defects. Mater. Des. **162**, 300–310 (2019). https://doi.org/10.1016/j.matdes.2018.11.060
4. Mathew, J.; Griffin, J.; Alamaniotis, M.; Kanarachos, S.; Fitzpatrick, M.E.: Prediction of welding residual stresses using machine learning: comparison between neural networks and neuro-fuzzy systems. Appl. Soft Comput. **70**, 131–146 (2018). https://doi.org/10.1016/j.asoc.2018.05.017
5. Das, D.; Pratihar, D.K.; Roy, G.G.; Pal, A.R.: Phenomenological model-based study on electron beam welding process, and input-output modeling using neural networks trained by back-propagation algorithm, genetic algorithms, particle swarm optimization algorithm and bat algorithm. Appl. Intell. **48**, 2698–2718 (2018). https://doi.org/10.1007/s10489-017-1101-2
6. Rai, R.; Palmer, T.A.; Elmer, J.W.; Debroy, T.: Heat transfer and fluid flow during electron beam welding of 304L stainless steel alloy. Weld. J. **88**, 54–61 (2009)
7. Vilar, R.; Zapata, J.; Ruiz, R.: An automatic system of classification of weld defects in radiographic images. NDT E Int. **42**, 467–476 (2009). https://doi.org/10.1016/j.ndteint.2009.02.004
8. Hou, W.; Wei, Y.; Jin, Y.; Zhu, C.: Deep features based on a DCNN model for classifying imbalanced weld flaw types. Measurement **131**, 482–489 (2019). https://doi.org/10.1016/j.measurement.2018.09.011
9. Lu, F.; Li, X.; Li, Z.; Tang, X.; Cui, H.: Formation and influence mechanism of keyhole-induced porosity in deep-penetration laser welding based on 3D transient modeling. Int. J. Heat

Mass Transf. **90**, 1143–1152 (2015). https://doi.org/10.1016/j.ijheatmasstransfer.2015.07.041
10. Deshpande, A.A.; Tanner, D.W.J.; Sun, W.; Hyde, T.H.; McCartney, G.: Combined butt joint welding and post weld heat treatment simulation using SYSWELD and ABAQUS. Proc. Inst. Mech. Eng. Part L J. Mater. Des. Appl. **225**, 1–10 (2011). https://doi.org/10.1177/14644207jmda349
11. Vourna, P.; Ktena, A.; Tsakiridis, P.E.; Hristoforou, E.: An accurate evaluation of the residual stress of welded electrical steels with magnetic Barkhausen noise. Measurement **71**, 31–45 (2015). https://doi.org/10.1016/j.measurement.2015.04.007
12. Akbari Mousavi, S.A.A.; Miresmaeili, R.: Experimental and numerical analyses of residual stress distributions in TIG welding process for 304L stainless steel. J. Mater. Process. Technol. **208**, 383–394 (2008). https://doi.org/10.1016/j.jmatprotec.2008.01.015
13. Paradowska, A.; Price, J.W.H.; Ibrahim, R.; Finlayson, T.: A neutron diffraction study of residual stress due to welding. J. Mater. Process. Technol. **164–165**, 1099–1105 (2005). https://doi.org/10.1016/j.jmatprotec.2005.02.092
14. Shi, J.; Booth, S.: An investigation of effects of welding residual stresses on creep crack growth for a low alloy butt weld. Int. J. Press. Vessel. Pip. **108–109**, 67–71 (2013). https://doi.org/10.1016/j.ijpvp.2013.04.010
15. Ferro, P.; Zambon, A.; Bonollo, F.: Investigation of electron-beam welding in wrought Inconel 706—experimental and numerical analysis. Mater. Sci. Eng. A **392**, 94–105 (2005). https://doi.org/10.1016/j.msea.2004.10.039
16. Reynolds, A.P.; Tang, W.; Gnaupel-Herold, T.; Prask, H.: Structure, properties, and residual stress of 304L stainless steel friction stir welds. Scr. Mater. **48**, 1289–1294 (2003). https://doi.org/10.1016/S1359-6462(03)00024-1
17. Liu, C.; Zhang, J.X.; Xue, C.B.: Numerical investigation on residual stress distribution and evolution during multipass narrow gap welding of thick-walled stainless steel pipes. Fusion Eng. Des. **86**, 288–295 (2011). https://doi.org/10.1016/j.fusengdes.2011.01.116
18. Huo, L.; Chen, F.; Zhang, Y.; Zhang, L.; Liu, F.; Chen, G.: 3D Finite element numerical simulation of residual stresses on electron beam welded BT20 plates. Cailiao Kexue Yu Jishu (J. Mater. Sci. Technol.) **20**, 117–120 (2004)
19. Thomas, K.; Arne, K.: Formation of welding residual stresses in low transformation temperature (LTT) materials. Soldag. Inspeção. **14**, 74–81 (2009). https://doi.org/10.1590/S0104-92242009000100009
20. Javadi, Y.; Pirzaman, H.S.; Raeisi, M.H.; Najafabadi, M.A.: Ultrasonic inspection of a welded stainless steel pipe to evaluate residual stresses through thickness. Mater. Des. **49**, 591–601 (2013). https://doi.org/10.1016/j.matdes.2013.02.050
21. Yelbay, H.I.; Cam, I.; Gur, C.H.: Non-destructive determination of residual stress state in steel weldments by magnetic Barkhausen noise technique. NDT E Int. **43**, 29–33 (2010). https://doi.org/10.1016/j.ndteint.2009.08.003
22. Barsoum, Z.; Barsoum, I.: Residual stress effects on fatigue life of welded structures using LEFM. Eng. Fail. Anal. **16**, 449–467 (2009). https://doi.org/10.1016/j.engfailanal.2008.06.017
23. Nguyen, N.T.; Ohta, A.; Matsuoka, K.; Suzuki, N.; Maeda, Y.: Analytical solutions for transient temperature of semi-infinite body subjected to 3-D moving heat sources. Weld. Res. Suppl. **78**, 265–274 (1999)
24. Nataraj, J.R.; Rajkumar, G.R.: Finite element analysis of dissimilar welding between newly developed Cr-free nickel based welding electrode and stainless steel AISI 304. Int. J. Res. Eng. Technol. **2**, 130–135 (2013)
25. Vemanaboina, H.; Akella, S.; Buddu, R.K.: Welding process simulation model for temperature and residual stress analysis. Procedia Mater. Sci. **6**, 1539–1546 (2014). https://doi.org/10.1016/j.mspro.2014.07.135
26. Bezerra, A.C.; Vieira, L.C.; Rade, D.A.; Scotti, A.: On the influence of welding residual stresses on the dynamic behavior of structures. Shock Vib. **15**, 447–458 (2008)
27. Kaldas, M.M.; Dickinson, S.M.: The flexural vibration of welded rectangular plates. J. Sound Vib. **75**, 163–178 (1981). https://doi.org/10.1016/0022-460X(81)90337-0
28. Jubb, J.E.M.; Phillips, I.G.; Becker, H.: Interrelation of structural stability, stiffness, residual stress and natural frequency. J. Sound Vib. **39**, 121–134 (1975). https://doi.org/10.1016/S0022-460X(75)80212-4
29. Kaldas, M.M.; Dickinson, S.M.: Vibration and buckling calculations for rectangular plates subject to complicated in-plane stress distributions by using numerical integration in a Rayleigh–Ritz analysis. J. Sound Vib. **75**, 151–162 (1981). https://doi.org/10.1016/0022-460X(81)90336-9
30. Gray, T.; Camilleri, D.; McPherson, N.: Control of Welding Distortion in Thin-Plate Fabrication, 1st edn. Woodhead Publishing Limited, Cambridge (2014)
31. Javadi, Y.; Smith, M.C.; Abburi Venkata, K.; Naveed, N.; Forsey, A.N.; Francis, J.A.; Ainsworth, R.A.; Truman, C.E.; Smith, D.J.; Hosseinzadeh, F.; Gungor, S.; Bouchard, P.J.; Dey, H.C.; Bhaduri, A.K.; Mahadevan, S.: Residual stress measurement round robin on an electron beam welded joint between austenitic stainless steel 316L(N) and ferritic steel P91. Int. J. Press. Vessels Pip. **154**, 41–57 (2017). https://doi.org/10.1016/j.ijpvp.2017.06.002
32. Xu, J.; Chen, J.; Duan, Y.; Yu, C.; Chen, J.; Lu, H.: Comparison of residual stress induced by TIG and LBW in girth weld of AISI 304 stainless steel pipes. J. Mater. Process. Technol. **248**, 178–184 (2017). https://doi.org/10.1016/j.jmatprotec.2017.05.014
33. Cullity, B.D.; Stock, S.R.: Elements of X-Ray Diffraction, 3rd edn. Pearson Education India, New Delhi (2014)
34. Rosenthal, D.: Mathematical theory of heat distribution during welding and cutting. Weld. J. **20**, 220–233 (1941)
35. Rosenthal, D.: The theory of moving sources of heat and its application to metal treatments. Trans. Am. Soc. Mech. Eng. **68**, 849–866 (1946)
36. Goldak, J.; Chakravarti, A.; Bibby, M.: A new finite element model for welding heat sources. Metall. Mater. Trans. B **15**, 299–305 (1984). https://doi.org/10.1007/BF02667333
37. Chang, W.S.; Na, S.J.: Prediction of laser-spot-weld shape by numerical analysis and neural network. Metall. Mater. Trans. B **32**, 723–731 (2001). https://doi.org/10.1007/s11663-001-0126-3
38. Prof. Gandham Phanikumar, Analysis and Modeling of Welding (Video), Heat sources part 2/2, NPTEL Video Lect. (2016). http://nptel.ac.in/courses/113106067/4
39. Luo, Y.; You, G.; Ye, H.; Liu, J.: Simulation on welding thermal effect of AZ61 magnesium alloy based on three-dimensional modeling of vacuum electron beam welding heat source. Vacuum **84**, 890–895 (2010). https://doi.org/10.1016/j.vacuum.2009.12.005
40. Das, D.; Pratihar, D.K.; Roy, G.G.: Electron beam melting of steel plates: temperature measurement using thermocouples and prediction through finite element analysis. In: Mandal, D.K., Syan, C.S. (eds.) CAD/CAM, Robotics and Factories of the Future, pp. 579–588. Springer, New Delhi (2016). https://doi.org/10.1007/978-81-322-2740-3_57
41. Podder, D.; Kenno, S.; Das, S.; Mandal, N.R.: Numerical investigation on interruption in the welding process used in shipbuilding. J. Ship Prod. Des. **31**, 220–229 (2015). https://doi.org/10.5957/JSPD.31.1.140005
42. Gery, D.; Long, H.; Maropoulos, P.: Effects of welding speed, energy input and heat source distribution on temperature variations in butt joint welding. J. Mater. Process. Technol. **167**, 393–401 (2005). https://doi.org/10.1016/j.jmatprotec.2005.06.018

43. Das, D.; Pratihar, D.K.; Roy, G.G.: Cooling rate predictions and its correlation with grain characteristics during electron beam welding of stainless steel. Int. J. Adv. Manuf. Technol. (2018). https://doi.org/10.1007/s00170-018-2095-6
44. Ranjbarnodeh, E.; Serajzadeh, S.; Kokabi, A.H.; Fischer, A.: Effect of welding parameters on residual stresses in dissimilar joint of stainless steel to carbon steel. J. Mater. Sci. **46**, 3225–3232 (2011). https://doi.org/10.1007/s10853-010-5207-8
45. Mohanty, S.; Laldas, C.K.; Roy, G.G.: A new model for keyhole mode laser welding using FLUENT. Trans. Indian Inst. Met. **65**, 459–466 (2012). https://doi.org/10.1007/s12666-012-0151-8
46. Shanmugam, N.S.; Buvanashekaran, G.; Sankaranarayanasamy, K.: Finite element simulation of Nd: YAG laser lap welding of AISI 304 stainless steel sheets. In: Arslan, O., Oprisan, S. (eds.) Recent Advances in Mechanical Engineering & Automatic Control, pp 174–179. Wseas LLC (2012)
47. Kazemi, K.; Goldak, J.A.: Numerical simulation of laser full penetration welding. Comput. Mater. Sci. **44**, 841–849 (2009). https://doi.org/10.1016/j.commatsci.2008.01.002
48. Chakraborty, S.S.; Maji, K.; Racherla, V.; Nath, A.K.: Investigation on laser forming of stainless steel sheets under coupling mechanism. Opt. Laser Technol. **71**, 29–44 (2015). https://doi.org/10.1016/j.optlastec.2015.02.013
49. Cheng, P.J.; Lin, S.C.: Analytical model to estimate angle formed by laser. J. Mater. Process. Technol. **108**, 314–319 (2001). https://doi.org/10.1016/S0924-0136(00)00858-X
50. Zhan, Y.; Zhang, E.; Ge, Y.; Liu, C.: Residual stress in laser welding of TC4 titanium alloy based on ultrasonic laser technology. Appl. Sci. **8**, 1997 (2018). https://doi.org/10.3390/app8101997
51. Shokri, V.; Sadeghi, S.; Sadeghi, M.H.; Javadi, Y.: Effect of heat input ratio on residual stress in multipass welding using finite element method and ultrasonic stress measurement. J. Nondestruct. Eval. **34**, 1–13 (2015). https://doi.org/10.1007/s10921-015-0301-0